Interaction of Transported Drugs with the Lipid Bilayer and P-Glycoprotein through a Solvation Exchange Mechanism

Hiroshi Omote and Marwan K. Al-Shawi
Department of Molecular Physiology and Biological Physics, University of Virginia Health System, Charlottesville, Virginia 22908-0736

ABSTRACT Broad substrate specificity of human P-glycoprotein (ABCB1) is an essential feature of multidrug resistance. Transport substrates of P-glycoprotein are mostly hydrophobic and many of them have net positive charge. These compounds partition into the membrane. Utilizing the energy of ATP hydrolysis, P-glycoprotein is thought to take up substrates from the cytoplasmic leaflet of the plasma membrane and to transport them to the outside of the cell. We examined this model by molecular dynamics simulation of the lipid bilayer, in the presence of transport substrates together with an atomic resolution structural model of P-glycoprotein. Taken together with previous electron paramagnetic resonance studies, the results suggest that most transported drugs are concentrated near the surface zone of the inner leaflet of the plasma membrane. Here the drugs can easily diffuse laterally into the drug-binding site of P-glycoprotein through an open cleft. It was concluded that the initial high-affinity drug-binding site was located in the interfacial surface area of P-glycoprotein in contact with the membrane interface. Based on these results and our recent kinetic studies, a "solvation exchange" drug transport mechanism of P-glycoprotein is discussed. A molecular basis for the improved colchicine transport efficiency by the much-studied colchicine-resistance G185V mutant human P-glycoprotein is also provided.

INTRODUCTION

Multidrug resistance (MDR) is a critical problem in cancer chemotherapy. Overexpression of P-glycoprotein (ABCB1, *MDR1* gene product) on the plasma membrane is frequently observed in drug-resistant cancer cells leading to the failure of chemotherapy (1). P-glycoprotein also modulates drug absorption, bioavailability, tissue disposition, and excretion and plays an important role in compromising AIDS chemotherapy and other drug-treatable diseases (reviewed in 2–4).

P-glycoprotein transports various hydrophobic compounds out of the cell by utilizing the energy of ATP hydrolysis (5). The amino acid sequence and topology of P-glycoprotein indicate that it is a member of one of the largest membrane protein families, namely the ATP binding cassette transporter family (ABC super family) (6). ABC transporters have two highly conserved ATP-binding catalytic domains and two relatively variable transmembrane domains that function together as a unit. These proteins play central roles in solute transport across various membranes. Transport substrates of ABC transporters include sugars, amino acids, vitamins, lipids, sterols, peptides, toxins, and drugs (7). A characteristic feature of P-glycoprotein is its broad substrate specificity (8). Typical transport substrates of P-glycoprotein are hydrophobic and positively charged molecules that can form hydrogen bonds (9–11). In many cases, these substrates have aromatic rings but this is not an absolute requirement. In general, P-glycoprotein does not transport net negatively charged compounds (reviewed in Seelig and Landwojtowicz (12)). Within these broad criteria, there are no further structural relationships between the diverse chemical compounds that P-glycoprotein transports. Such a diversity of P-glycoprotein substrates poses a significant problem for clinical treatment. Therefore, elucidating the mechanism of substrate recognition by P-glycoprotein is of great medical interest.

P-glycoprotein substrates generally partition to the lipid bilayer due to their hydrophobicity. When photoactivated, photoreactive drugs label the transmembrane domain of P-glycoprotein, indicating that substrate binding sites are located in the membrane region (13,14). In addition, mutations in the transmembrane domains change the substrate specificity (15,16). Interestingly, the apparent K_m values of P-glycoprotein drugs have a clear correlation with the hydrophobicity of these drugs (12). Based on such studies, Gottesman and colleagues postulated the ''hydrophobic vacuum cleaner model'' (1). In this model, hydrophobic drugs are partitioned into the inner leaflet of the plasma membrane where P-glycoprotein takes these drugs from the lipid bilayer and transports to the aqueous phase of the other side of membrane. This model was supported by transport experiments with fluorescent drugs (17–20) and more recently by EPR studies employing spin-labeled verapamil (21). However, despite the extensive biochemical and genetic studies, details of drug recognition by the P-glycoprotein remain obscure. A common theme emerging from the studies discussed above was that the interaction of drugs with the lipid bilayer was a primary determinant for substrate recognition of P-glycoprotein. Consequently, substrate

Submitted November 14, 2005, and accepted for publication January 4, 2006.

Address reprint requests to Marwan K. Al-Shawi, Dept. of Molecular Physiology and Biological Physics, University of Virginia Health System, PO Box 800736, Charlottesville, VA 22908-0736. Tel.: 434-243-8674; Fax: 434-982-1616; E-mail: ma9a@virginia.edu.

Hiroshi Omote's present address is Dept. of Membrane Biochemistry, Faculty of Pharmaceutical Sciences, Okayama University, 1-1-1 Tsushimanaka, Okayama 700-8520, Japan.

0006-3495/06/06/4046/14 $2.00

doi: 10.1529/biophysj.105.077743

binding by P-glycoprotein should be considered in two steps, the initial partitioning of drugs to the lipid bilayer followed by binding to transmembrane region of P-glycoprotein (21). Recent progress in molecular dynamics (MD) simulations allows the simulation and investigation of the interactions of small molecules with the lipid bilayer (22–24). In this study, we tested the interaction of P-glycoprotein transport substrates with the lipid bilayer by molecular dynamics and explored possible drug-recognition sites by atomic detail homology modeling of human P-glycoprotein.

MATERIALS AND METHODS

Molecular dynamics simulations

Topology and coordinates of each drug were generated by PRODRG (25). For charged molecules, the charge distribution was calculated using MOPAC (26). Charged rhodamine 123, daunorubicin, protonated verapamil, and spin-labeled verapamil (SL-verapamil, (21)) were treated as having a +1 charge and Hoechst 33342 was treated as having a +3 charge. Coordinates and parameters for dipalmitoyl phosphatidylcholine (DPPC) were obtained from previous reports (27,28). Simulations were run using the GROMACS v3.14 with a modified GROMOS87 force field, parameter set *ffgmx* (29,30).

Energy minimized drug molecules were manually placed on the surface area of the lipid bilayer. For positively charged drugs, chloride anions were added to keep the net charge of the system neutral. To minimize the artifact of a periodic boundary, the lipid bilayer was fully hydrated by simple point of charge water molecules at a water/lipid ratio of 33 or larger (27). A typical system contained 128 molecules of DPPC, 1 drug molecule, and ~4625 water molecules with initial dimensions of 6.42 × 6.44 × 7.50 nm. The system temperature was set to 325 K, well above the transition temperature of the DPPC bilayer. Systems were subjected to 1000 steps of steepest descents energy minimization followed by 100 ps molecular dynamics. The resultant coordinates were used for 10–20 ns molecular dynamics simulations. These simulations were carried out in the NPT ensemble with constant pressure (1 bar) for all three directions using a coupling constant of $\tau_P = 1.0$ ps. Temperatures of lipids, water, and drugs were controlled separately with a temperature-coupling constant of $\tau_T = 0.1$ ps. All bond lengths were constrained using LINCS (31). A twin-range cutoff of 0.9–1.8 nm was used for Lennard-Jones (van der Waals) and long-range electrostatic interactions, respectively. Integration step time was 2 fs and trajectories (coordinates and velocities) were recorded each 20 ps. In this configuration, the system was stable for at least 20 ns. All simulations were carried out a minimum of two times.

Homology modeling of human P-glycoprotein

Homology modeling of human P-glycoprotein was carried out using MODELLER 6v3 (32) by a new refined procedure of our previously described method (33). Transmembrane regions and nucleotide binding domains were modeled separately in an approach similar to that previously reported for MsbA (34). Initially, sequences of *Vibrio cholera* MsbA (residues 10–564), human P-glycoprotein N-terminal half (residues 34–637), and C-terminal half (residues 694–1279) were aligned through ClustalX (35). Alignment of transmembrane domains was verified by secondary structure analysis (PHD (36) and PROF (37)) and then manually adjusted by the location of gaps and aromatic residues. The crystal structure of *V. cholera* lipid A transporter MsbA (Protein Data Bank (PDB) file 1PF4) was used as a template structure for the transmembrane domains (38). Missing parts of the crystal structure (residues 203–237 of MsbA, and residues 250–284 and 893–927 of human P-glycoprotein) were each modeled as a helix-loop-helix as predicted by PHD (Fig. 1). The conformation of *V. cholera* MsbA nucleotide-binding domain was different from other ABC proteins. In MsbA, the catalytic P-loop (Walker A motif) was not aligned with other catalytic residues such as Asp-505, Glu-506 of the Walker B motif (MsbA numbering), or the Q-loop. This suggested that catalytic domain of this crystal structure was not in an active form. Therefore, P-glycoprotein nucleotide binding domains (residues 340–637 and 983–1280) were modeled using *Salmonella typhimurium* histidine permease HisP coordinates (PDB file 1B0U) as a template structure (39). Modeled P-glycoprotein nucleotide binding domains (residues 391–637, 1034–1280) and transmembrane domains (10–390, 695–1033) were assembled by fitting to the corresponding regions of the MsbA structure. The linker regions (P-glycoprotein residues 360–390 and 1014–1035) between transmembrane domains and nucleotide binding domains did not fit the MsbA structure. These regions were modeled as a helix and a loop according to secondary structure prediction. PROCHECK (40) was used to check for atom clashes, bond lengths, adequate bond angles, and backbone dihedral stereochemistry. When unfavorable conditions were encountered, molecular dynamics simulated annealing was performed using MODELLER. The temperature was increased from 150 to 1300 K in six steps with 300 iterations each for equilibration followed by nine cooling steps to 300 K with 1000 iterations each for equilibration. This intermediate model contained some atomic clashes, particularly in the Walker B regions, that could not be resolved by energy minimization alone. To overcome this, the nucleotide binding domains (residues 340–637 and 983–1280) were remodeled into this intermediate form using human TAP1 (41) as a template (PDB file 1JJ7). Initially, there were still small atomic conflicts between the Walker B regions. These conflicts disappeared after a few cycles of energy minimization as described above. The final model had no atom clashes and generated a Ramachandran plot (42) in which 98.7% of the backbone angles were in allowed regions. Coordinates are available by request. It is important to note that the final structure recapitulated the ''nucleotide sandwich'' dimer-interface seen in *Escherichia coli* BtuCD (43) (PDB file 1L7V) although this structure was not used in the modeling (see Fig. 2 *B*). The BtuCD nucleotide dimer interface is believed to be a physiologically relevant form (44).

Fig. 1 illustrates the location of structural elements and conserved motifs in the primary sequence of human P-glycoprotein. The resultant modeled structure is shown in Fig. 2. As discussed in Omote et al. (33) the structural model generated was different from that of Seigneuret and Garnier-Suillerot (45), which was in an open conformation. The model of Fig. 2 was in a closed conformation and was similar to the structural models of Stenham et al. (46) and more recently Pleban et al. (14). Both of these later models demonstrated the presence of a central cavity as was observed in Fig. 2. The nucleotide binding-site dimer interface (Fig. 2 *B*) was similar to that of Shilling et al. (47). For a review of the dimer interface see Higgins and Linton (48). The order of transmembrane helices (TM) (Fig. 2 *C*) was 2, 3, 4, 1, 6, 5, 8, 9, 10, 7, 12, 11; counterclockwise when viewed from the cytoplasm. Recent cross-linking experiments have verified this order (49,50). This same order of TMs was also observed in the recent x-ray crystal structure of *S. typhimurium* MsbA (51). Overall, the model presented in Fig. 2 is a consensus structural model that is expected to be highly representative of the true structure of P-glycoprotein.

Measurement of intrinsic drug transport turnover numbers

The intrinsic turnover numbers for drug transport at pH 7.5 and 35°C were obtained for the transport of verapamil, spin-labeled verapamil, Hoechst 33342, colchicine, rhodamine 123, and daunorubicin by human P-glycoprotein reconstituted into ''mixed lipid'' proteoliposomes (52). The methods employed are fully described in Omote et al. (33). Briefly, P-glycoprotein

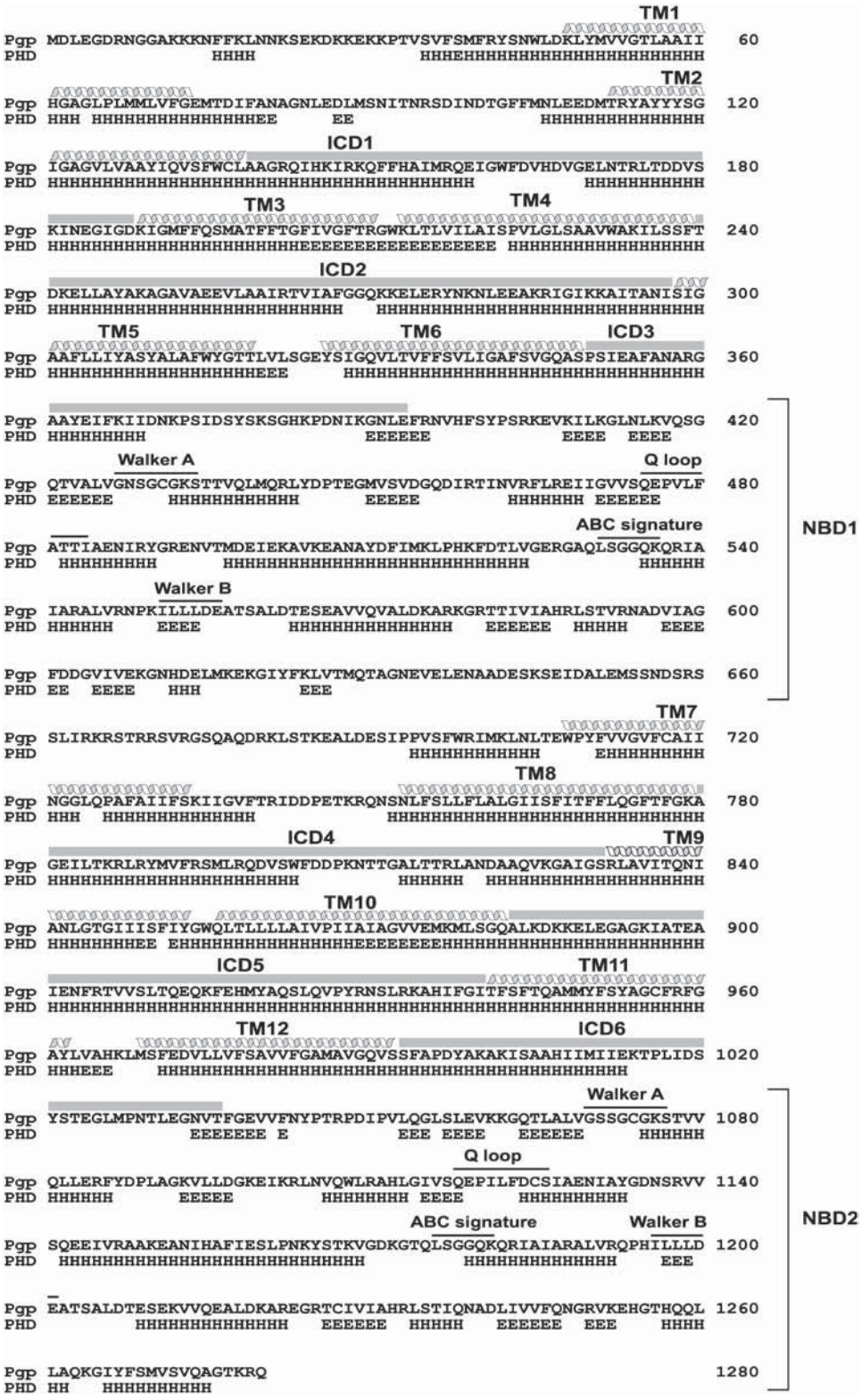

FIGURE 1 Location of structural elements and conserved motifs in the primary sequence of human P-glycoprotein. The primary sequence of human P-glycoprotein is shown with the PHD predicted secondary structure (37) where H indicates helical residues and E indicates β-strand residues. Locations of transmembrane residues (TM1–TM12) are indicated by ribbon helices and locations of intracellular domains are indicated by shaded bars (ICD1–ICD6) (based on Chang (38)). Conserved nucleotide binding domain (*NBD*) motifs Walker A, Q-loop, ABC signature, and Walker B are indicated by solid black bars.

turnover numbers were measured as a function of drug concentration, ATP concentration, and seven temperatures by Pi production rates of ATP hydrolysis. For conditions of coupled drug transport, the intrinsic V_{max} values at saturating ligand concentrations were calculated by extrapolation of the kinetic and thermodynamic data obtained to saturating drug and ATP concentrations. The turnover number for the flux through the coupled drug transport cycle (52) was equated to the intrinsic drug transport rate of P-glycoprotein.

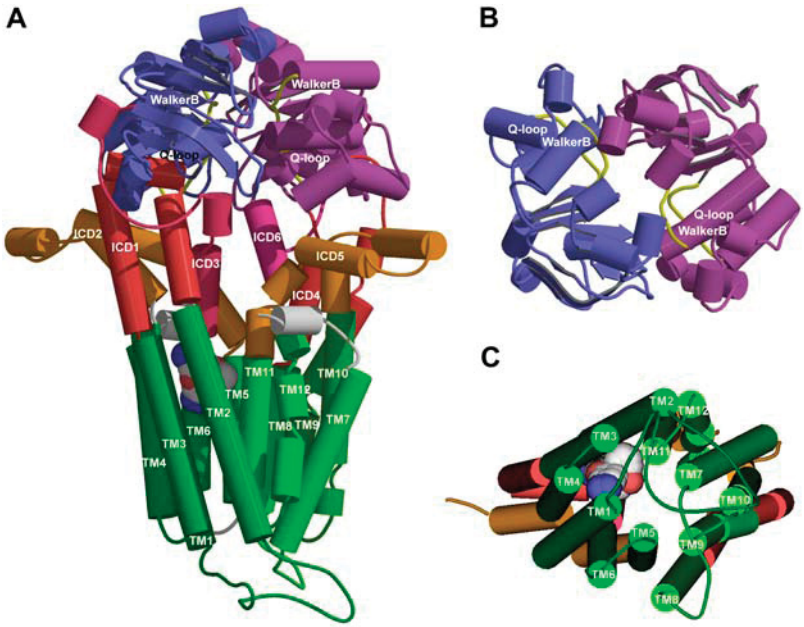

FIGURE 2 Atomic detail homology and energy minimized model structure of human P-glycoprotein. This model is a refinement of our previous homology model (33). The crystal structure coordinates of *V. cholera* lipid A transporter MsbA (38) *S. typhimurium* histidine permease HisP (39) and human TAP1 (41) were used (see Materials and Methods). Atom conflicts were removed by simulated annealing and the structure was energy minimized. One rhodamine 123 molecule (illustrated by *space-filling model*) is shown in the putative high-affinity binding site of the N-terminal half-molecule. See text for further details. (*A*) A closed-structure conformation of the whole protein and bound drug showing discussed structural elements. (*B*) View of the nucleotide sites from the cytoplasm. (*C*) View of the TMs from outside the cell, illustrating the drug binding structures.

RESULTS

Drug and lipid bilayer interactions investigated by molecular dynamics

In this study, dipalmitoyl phosphatidylcholine was chosen because membrane bilayers with this lipid have been well characterized by molecular dynamics studies (27). In addition, P-glycoprotein is believed to be enriched in lipid rafts containing saturated lipids (53). There were no significant drifts of pressure, temperature, and box size over the 10–20 ns simulations suggesting that the lipid bilayer was well equilibrated. The mean distance between lipid phosphorous atoms of the two leaflets was 3.9 nm and the surface area per lipid was 0.64 nm^2. Values were slightly larger than those reported previously (27) due to the higher temperature employed here. We tested deprotonated verapamil, protonated verapamil, Hoechst 33342, spin-labeled verapamil (SL-verapamil, (21)), colchicine, charged and uncharged forms of rhodamine 123, and daunorubicin, for drug-lipid interactions. All of these drugs are good transport substrates of P-glycoprotein for which kinetic and thermodynamic data are available (52). The structures of these drugs are shown in Fig. 3. Typical snapshots after 10 ns of simulation are illustrated in Fig. 4 for deprotonated and protonated forms of verapamil. Trajectory analysis of deprotonated verapamil showed two different phases (Fig. 5, *A* and *B*). Until ~5 ns deprotonated verapamil was located in the surface area of the lipid bilayer, then suddenly it entered into the hydrocarbon core of the lipid bilayer (Figs. 4 *A* and 5 *A*, *z* axis). Except for the transition, the *z* axis position of verapamil was then stable. On the other hand, movement parallel to the membrane (lateral diffusion) was free until the end of the simulation time course. Similar patterns were observed in multiple simulation runs. This result indicates that deprotonated verapamil has two different phases of lipid interaction and there is an energetic barrier to enter the hydrophobic core of the membrane. Flip-flop of deprotonated verapamil was not observed during the 20 ns time courses, suggesting there is another energy barrier to cross to the other side of the bilayer. Such a flip-flop is expected to occur in a much longer time domain (54). However, portions of the verapamil molecules were observed to cross the membrane median (Fig. 6 *A*). For the other drugs simulated, entry deep inside the hydrocarbon zone without surface interaction was not observed (Figs. 4 *B*, 5 *B*, and 6 *B–F*). For these drugs, vertical movement was limited in the membrane (*Z* axis) after establishing stable lipid interactions. On the other hand, lateral diffusion occurred freely in the *X* and *Y* plane.

Atomic and molecular density distributions after establishment of stable drug-lipid interactions are summarized in Fig. 6. The averaged equilibrium positions from the center of the bilayer for the different drugs were as follows: deprotonated verpamil, 0.73 nm; protonated verapamil, 1.47 nm; Hoechst 33342, 1.46 nm; SL-verapamil, 1.49 nm; colchicine, 1.41 nm; uncharged rhodamine 123, 1.45 nm; charged rhodamine 123, 2.03 nm; and charged daunorubicin, 2.08 nm. Clearly, the drugs prefer the surface or interfacial region of the membrane except for deprotonated verapamil. In general, the hydrophobic part of the drugs enters the hydrocarbon zone of the lipid bilayer but the charged part maintains interactions with the surface (Fig. 4 *B*). On entering the hydrocarbon layer of the lipid bilayer, deprotonated verapamil lost all H-bonds (Fig. 5 *C*). In contrast, the protonated form maintained H-bonds to water and lipid headgroups throughout the simulation time (Fig. 5 *D*). The protonated nitrogen of verapamil formed hydrogen bonds to

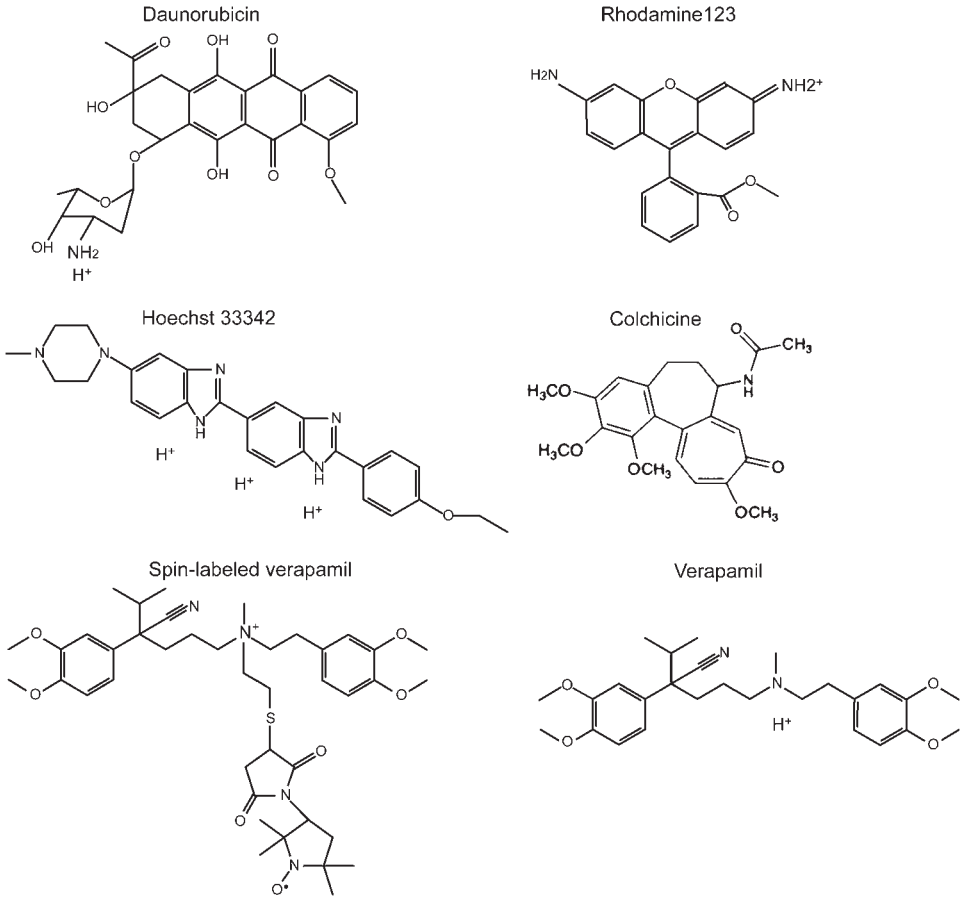

FIGURE 3 Chemical structures of drug molecules used in molecular dynamics simulations.

oxygen atoms of carbonyl, phosphate, and glycerol moieties of the lipid. Although the number of polar interactions with the surface interfacial zone was different for each drug, similar patterns were observed for the other cationic drugs (not shown).

Drug recognition site of human P-glycoprotein

Bacterial lipid A transporters (MsbA) are members of the ABC protein family and exhibit high homology to human P-glycoprotein. Expression of MsbA in *E. coli* conferred multidrug resistance and ethidium extrusion to the cells. Additionally purified and reconstituted protein was shown to bind drugs and to transport Hoechst 33342, suggesting that MsbA works, to some extent, as a drug transporter (55). Moreover, one member of the P-glycoprotein family, MDR3 (ABCB4), transports phosphatidylcholine (56). Given the functional similarity and high degree of homology of *E. coli* MsbA and P-glycoprotein (31% and 30% sequence identity with the N- and C-terminal halves, respectively), we can expect that they share a similar structure and mechanism. It has been demonstrated that proteins with a sequence identity greater than 25% have similar three-dimensional structures (57). Recent crystal structures of *E. coli* and *V. cholera* MsbA showed that it contained an internal large chamber enclosed by the transmembrane domains from each half-molecule. This chamber has enough space to bind lipid A (38,58). A unique distribution of positive charges inside the chamber insinuated the importance of charged residues in the transmembrane region for substrate recognition of the negatively charged lipid A. As the crystal structure of human

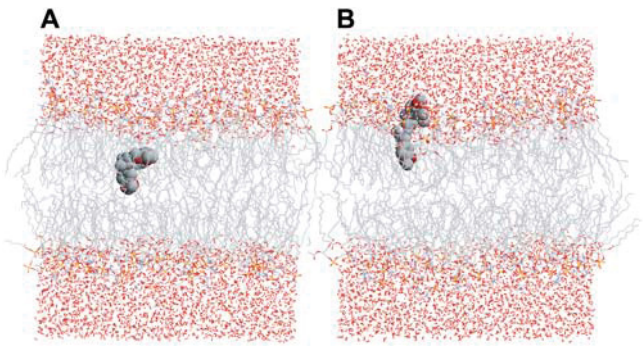

FIGURE 4 Snap shots from molecular dynamics simulations. Snapshots of deprotonated verapamil (*A*) and protonated verapamil (*B*) were taken at the end of 10 ns molecular dynamics simulations. Drugs are illustrated by large space-filling models, water molecules by small ball models and lipids by line models.

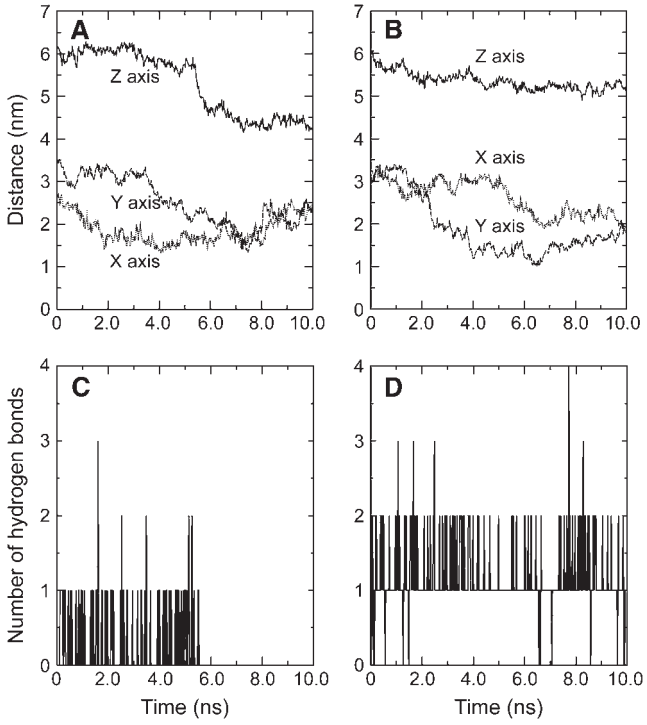

FIGURE 5 Trajectory and hydrogen bond formation of verapamil in the membrane bilayer. Molecular dynamics simulations of P-glycoprotein transport drugs entering a DPPC bilayer were performed as detailed in Materials and Methods. Centers of mass of deprotonated verapamil and protonated verapamil were calculated and plotted against the elapsed simulation time. Distances for each axis were measured from the corner of the simulation box. *X* and *Y* axes are parallel to the plane of the membrane and the *Z* axis is perpendicular to the lipid bilayer. The center of the lipid bilayer in the *Z* axis is 3.74 nm. (*A*) Illustrates the change in coordinate distances for deprotonated verapamil. (*B*) Illustrates the change in coordinate distances for protonated verapamil. Hydrogen bonds formed between verapamil and water and lipid headgroups were also determined during the simulation time course. Number of hydrogen bonds formed is plotted as a function of time for deprotonated verapamil (*C*) and protonated verapamil (*D*). In panel *C*, after 5.5 ns, deprotonated verapamil fully enters the hydrocarbon core of the bilayer and abolishes all hydrogen bonding from then on (zero hydrogen bonds formed).

P-glycoprotein is still not available, we examined the possible drug binding site of this protein based on a modified version (Materials and Methods) of a homology modeled structure (33) constructed using *V. cholera* MsbA (38), *S. typhimurium* HisP (39), and human TAP1 (41).

P-glycoprotein favors positively charged amphipathic molecules (see Introduction), which suggests the involvement of acidic residues in drug binding. Interestingly, there were no acidic residues in the chamber of the modeled structure indicating cationic selectivity of P-glycoprotein is not determined by this region (see Figs. 7 and 8). In MsbA the chamber carries a net positive charge (38,58). In models of P-glycoprotein the net charge of the chamber is weak and may be slightly positive (Fig. 8). However, the outside perimeter of the intracellular domain helices (ICD helices of Fig. 2 *A*, located above the membrane in Fig. 7) has strong positive charge densities (not shown). On the other hand, there are well-conserved acidic residues in the surface zone of the chamber and helix bundle composed of ICD helices 1, 3, 4, and 6 (Fig. 7, *shaded labels*; see also Fig. 1 for alignments). These residues, D188, E353, E782, and D997 are close to the membrane surface and facing inside the ICD bundle. Furthermore, these residues are accessible from within the putative drug-binding chamber. Thus, these residues are in a good position to form electrostatic interactions with positively charged drugs that enter the chamber. Since cationic drugs are concentrated in the surface area of membrane (Fig. 6), these residues may contribute to the positive charge drug selectivity of P-glycoprotein. Recent data obtained for E314 of LmrA (59), a homologous residue of residues E353 and D997 of P-glycoprotein, are supportive of this notion. In the same region, many other hydrophilic residues can form H-bonds with drugs. These residues include Q132, Q143, Q195, S196, T199, S228, K234, N296, S309, Q347, S351, and N357 in the N-terminal half-molecule (Fig. 7 *A*) and residues Q773, T776, T785, S831, Q838, N839, N842, S880, K877, Q990, and S993 in the C-terminal half-molecule (Fig. 7 *B*). Also, many aromatic residues such as F135, W136, W232, Y310, F343 in the N-terminal half (Fig. 7 *A*) and F777, F942, Y953, and F994 in the C-terminal half (Fig. 7 *B*) were found in the chamber near these acidic residues. Side chains of aromatic residues contribute to drug binding through interaction with the aromatic rings of drugs (60). These types of interactions have been observed in the AcrB multidrug efflux pump of *E. coli* (61). Such aromatic residues are not conserved in MsbA. The many polar residues scattered throughout the putative drug-binding chamber (Fig. 7) serve to form hydrogen bonds with drugs and water. Such hydrophilicity of the chamber appears to be a critical feature of P-glycoprotein functionality as discussed later. The interaction of drugs with P-glycoprotein through hydrogen-bond donor side chains and clusters of amino acids with π-electron systems has been previously proposed (62).

To test the proposed involvement of the chamber residues discussed above in drug binding, we performed MD simulations using the modeled structure generated. GROMACS v3.14 was used for simulations as previously discussed. Water molecules were introduced into the putative drug-binding chamber by the GENBOX function. A single molecule of rhodamine 123 was manually introduced into the chamber and MD simulations were run. An equilibrium drug-binding position was found. Rhodamine 123 xanthenyl-moiety was found to interact with the aromatic residues W136 and F200 through van der Waals interactions. Similarly, the benzoic acid moiety interacted with residue F343 through van der Waals interactions. Residue K234 formed an H-bond to the carbonyl of the benzoic acid methyl ester. Residue M192 and Q195 were also involved in forming the binding site. Additionally the rhodamine 123 molecule oscillated forming from zero to two transient H-bonds with

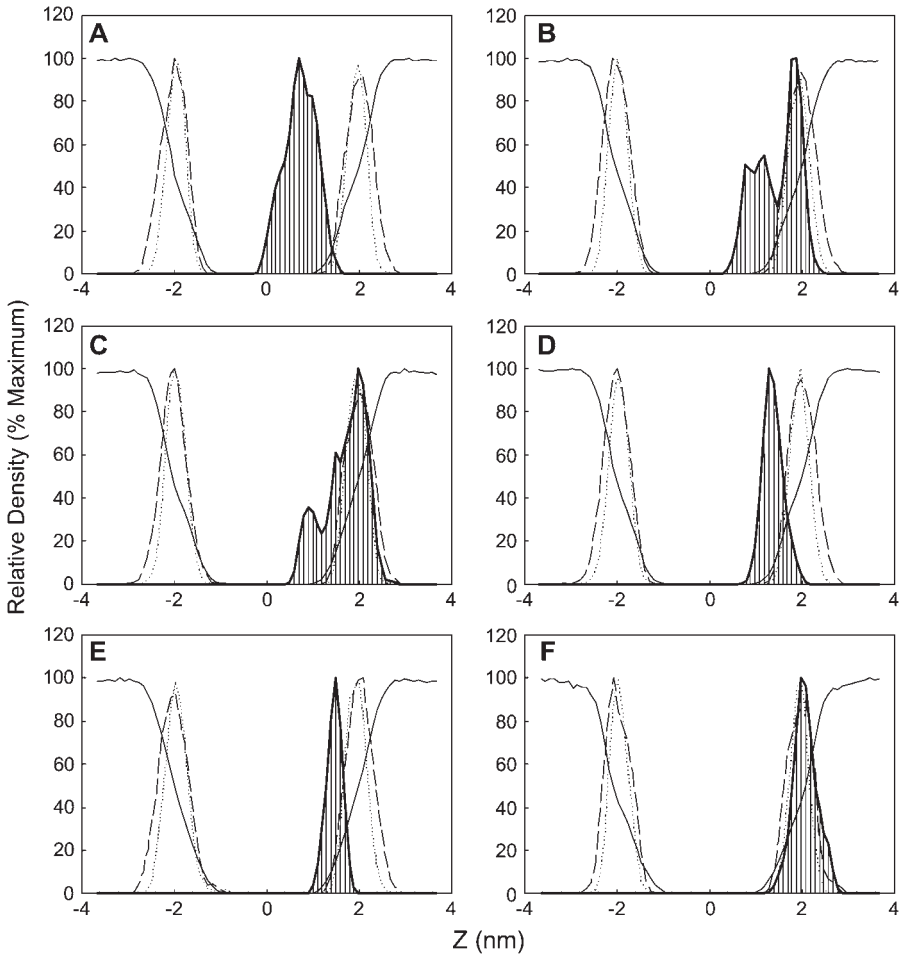

FIGURE 6 Distribution density profiles of drugs across the lipid bilayer. Distribution density profiles relative to maximum distribution values of drugs, water and lipid atoms were plotted against the *Z* axis position from the center of the membrane. Positive *Z* axis values represent distances from the center of the bilayer toward the cytoplasm whereas negative values are distances toward the outside of the cell. Averaged densities were taken from MD trajectories after reaching stable equilibrium positions (7–10 ns averaged). (*A*) Deprotonated verapamil; (*B*) protonated verapamil; (*C*) Hoechst 33342; (*D*) SL-verapamil (colchicine very similar, not shown); (*E*) uncharged rhodamine 123; (*F*) charged daunorubicin (charged rhodamine superimposable). Distribution density lines are: thick solid lines with hatched areas, drug; solid lines, water; dotted lines, phosphorous atoms of DPPC; dashed lines, nitrogen atoms of DPPC.

residues Q195, S196, T199, L227 (main-chain carbonyl), and S228. Similar interactions were observed by extensive molecular dynamics simulations when the modeled P-glycoprotein was inserted into a fully hydrated POPC bilayer containing 448 POPC lipids in the presence of 100 mM NaCl (H. Omote and M. K. Al-Shawi, unpublished data). These results confirm the importance of the aromatic and polar chamber residues in drug binding and indicate a degree of flexibility in drug binding by P-glycoprotein. In the simulations it was found that the average distances from the center of the rhodamine 123 molecule to the Walker A conserved lysine ε-amino nitrogen atoms were 46 Å and 45 Å for residues K536 and K1076, respectively. These lysine ε-amino nitrogen atoms were only 10.5 Å apart after rhodamine 123 binding. Sharom and colleagues (63,64) measured somewhat smaller distances of 38 Å, by a fluorescence resonance energy transfer (FRET) approach, from the nucleotide sites to bound rhodamine 123 (fluorescence donor). It is likely that the large fluorescence acceptor moieties (7-cholo-4-nitorbenz-2-oxa 1,2-diazole), covalently attached to the conserved C428 and C1071 of the Walker A sequence of Chinese hamster P-glycoprotein, account for the apparent shorter distances to the rhodamine 123 binding site.

Contribution of hydrogen bonds to drug specificity and transport turnover rates

For charged drug species, MD simulations showed that potential hydrogen bonds could not be satisfied within the hydrocarbon layer of the bilayer (Figs. 4 and 5). Thus, it appears that one function of P-glycoprotein is to provide alternative hydrogen bonds to drugs. P-glycoprotein must pick up the drugs at the membrane/water interface where they were located (Fig. 6, *B–F*). Hence, as discussed above, P-glycoprotein must have some hydrophilic residues to interact with drugs near the lipid surface for hydrogen bond exchange. To study this involvement of H-bond donation by P-glycoprotein, we plotted a free energy relationship between the experimentally determined intrinsic drug transport rate and the MD calculated number of H-bonds formed with the drug (Fig. 9). The log value of the time-averaged number of H-bonds formed by a drug is directly proportional to the potential H-bonding interaction-energy available.

There was a direct linear free energy relationship between the potential of the drug to form H-bonds and the intrinsic drug transport rate of P-glycoprotein (Fig. 9). For drugs with a high H-bonding potential the intrinsic transport rate was

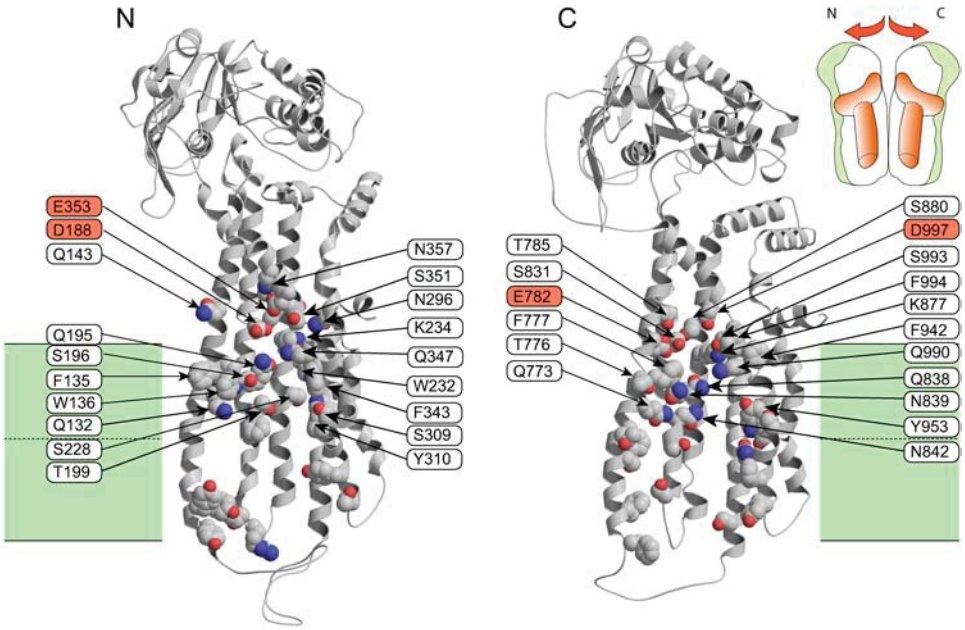

FIGURE 7 Postulated P-glycoprotein residues that contribute to initial drug binding. A structural model of human P-glycoprotein is shown based on homology modeling (Fig. 2). See Materials and Methods for modeling details. Amino terminal and carboxyl terminal halves of P-glycoprotein molecules are illustrated in left and right side panels, respectively. Both half-molecules are viewed parallel to the plane of the membrane from the center of the putative drug chamber side as illustrated by the schematic inset. A whole P-glycoprotein molecule can be assembled by rotating one of the two halves by 180° normal to the plane of the membrane and bringing the two halves together to form the putative drug binding chamber. The membrane zone is shown as green bands with a dotted line indicating the center of the bilayer. Polar and aromatic residues inside the chamber are illustrated by space filling models. Candidate residues that contribute to initial drug binding are labeled by arrows. Negatively charged residues have shaded labels. Structure illustrations were prepared by Molscript (89).

slow (e.g., daunorubicin). Whereas for drugs with a low H-bonding potential the intrinsic drug transport rate was fast (e.g., SL-verapamil). As discussed later, the flipping of a drug in P-glycoprotein's drug-binding chamber becomes harder with more H-bonds that need to be broken and reformed. This inverse relationship between drug H-bonding potential and turnover rate of P-glycoprotein has been previously observed (12,65).

Wild-type (WT) P-glycoprotein behaved anomalously by transporting colchicine too slowly relative to its H-bonding potential. The G185V mutation suppresses this effect by increasing the intrinsic rate of transport to the expected one (Fig. 9). It should be emphasized that G185V P-glycoprotein does not change the intrinsic drug transport rate or drug binding characteristics of all drugs but only a limited subset such as colchicine and etoposide (33). This suggests that a specific colchicine and etoposide drug-binding site has been altered by mutation and not the other drug-binding sites, and implies the existence of multiple chemically distinct drug-binding sites on P-glycoprotein. Thus, the G185V mutation distorts the binding site for colchicine while leaving binding sites of other drugs intact. Binding of colchicine to WT and G185V P-glycoproteins were characterized by van't Hoff analysis by methods previously described (52). For WT P-glycoprotein the thermodynamic parameters $\Delta H°$, $T\Delta S°$, and $\Delta G°$ of colchicine binding at 35°C and pH 7.5 were +25.7, +44.0, and −18.3 kJ mol^{-1}, respectively. Thus, the net driving force for colchicine binding to WT protein was through hydrophobic interactions (favorable entropy term). The corresponding values for colchicine binding to G185V P-glycoprotein were −191.4, −176.9, and −14.5 kJ mol^{-1}, respectively. Here the net driving force for colchicine binding to G185V P-glycoprotein was through favorable noncovalent interactions (H-bonds) compensated somewhat by a large unfavorable entropy term. Such net favorable noncovalent interactions compensated by an unfavorable entropy term have been previously characterized for verapamil

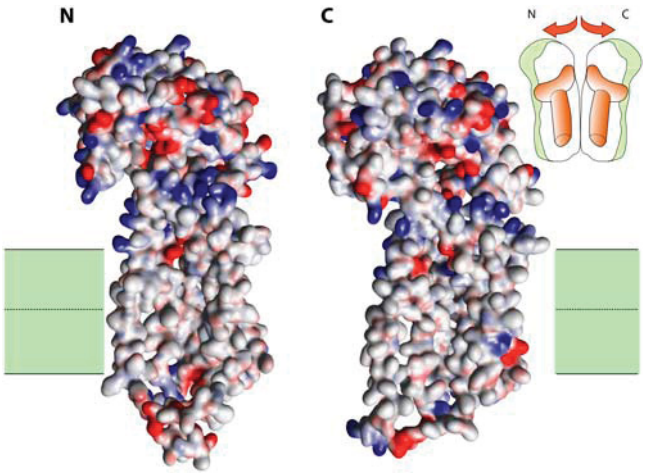

FIGURE 8 Surface potential distribution of modeled human P-glycoprotein. A molecular surface of modeled human P-glycoprotein showing the electrostatic potential distribution is shown in the same orientation as Fig. 7. The figure was prepared with WebLab ViewerPro (Accelrys, San Diego, CA) with red and blue indicating negative and positive charge, respectively.

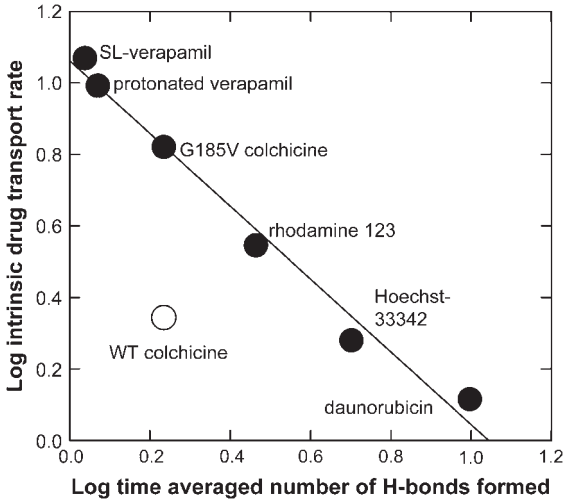

FIGURE 9 Drug hydrogen bond formation correlates with P-glycoprotein drug transport activity. The log of experimentally determined intrinsic drug transport rates was plotted against the log of MD simulated time-averaged number of H-bonds formed between the drug and the lipids at equilibrium. For drug transport activity assays, pure human P-glycoprotein reconstituted in ''mixed lipid'' proteoliposomes was assayed at 35°C and pH 7.5 (see Materials and Methods section for details). The line plotted was a linear regression fit to the data excluding the colchicine interaction with wild-type (*WT*) P-glycoprotein (*open symbol*). The linear free energy relationship was characterized by a slope of −1.018, an intercept of 1.063, and an R^2 value of 0.9814.

binding to WT P-glycoprotein (52). The results above indicate that, in WT P-glycoprotein, colchicine was binding too tightly to the ground state through specific nonpolar van der Waals interactions leading to a decreased transport rate. The G185V mutation modified the colchicine binding site in such a fashion as to reduce the contribution of nonpolar interactions. Polar interactions were now dominant and the overall colchicine affinity was reduced. These factors improve the colchicine transport rate and coupling efficiency of the G185V mutation as previously described (33).

DISCUSSION

The most remarkable features of P-glycoprotein are its broad transport-substrate specificity and the existence of basal ATPase activity in the absence of drug substrates (52). These features suggest that bond interactions between drugs and P-glycoprotein required to trigger the ATPase reaction exhibit a high degree of flexibility. The observed broad drug-specificity is an essential component of P-glycoprotein's function as a multidrug resistance pump. Thus, a good understanding of substrate recognition by P-glycoprotein is of primary interest in drug development for the treatment of cancer, AIDS, and other diseases influenced by P-glycoprotein.

Drug and membrane interactions

Most P-glycoprotein substrates are hydrophobic and are concentrated in the membrane. Even in the case of SL-verapamil, a relatively hydrophilic drug, the concentration in the vesicle membranes was 11 times higher than the concentration in the bulk water phase (21). A clear relationship between the partition coefficient of drugs and the apparent K_m for drugs by P-glycoprotein exists (12,66). Such results indicate that drug binding to the lipid bilayer is an initial step of drug recognition by P-glycoprotein. In this regard, the mode of interaction of drugs with the lipid bilayer is an important property to understand. Results of MD simulations performed in this study showed that cationic P-glycoprotein drugs were concentrated in the surface zone of the membrane (Fig. 6). Hydrophobic parts of the drug molecules were able to enter the hydrocarbon core of the membrane, but the drugs simultaneously retained polar interactions with water and lipid headgroups (see Results). Thus, polar interactions of drugs and lipid headgroups need to be considered.

Recently, we described a new spin-labeled verapamil, which was an excellent transport substrate of P-glycoprotein, and was relatively hydrophilic due to a fixed positive charge (21). Partition coefficients of SL-verapamil between water and olive oil showed that it was 120-fold more hydrophilic than verapamil. Despite such hydrophilicity, P-glycoprotein has a higher affinity and transport rate for SL-verapamil than for verapamil. According to the classical ''hydrophobic vacuum cleaner model'' (1), a hydrophilic molecule is expected to have a lower affinity to P-glycoprotein. The high apparent affinity of SL-verapamil for P-glycoprotein seems to violate this rule. A likely explanation of this apparent discrepancy is that the true substrate of P-glycoprotein is the protonated form of verapamil that is taken up from the surface zone (Fig. 6 *B*). In MD simulations, protonated verapamil was located near the surface region of membrane due to the polar interaction with lipid headgroups and water (Figs. 4 *B* and 6 *B*). The results of Fig. 9 confirm that protonated verapamil is the transported entity.

SL-verapamil never fully enters the hydrophobic core of the membrane (Fig. 6 *D*). In agreement with this, doxorubicin, another cationic P-glycoprotein substrate was reported as being located in the surface area of bilayers by fluorescence quenching experiments (67). The predominant species of rhodamine 123 is a protonated form, since the estimated pK_a is 11 (68,69). In our simulations, protonated rhodamine 123 was located near the surface region of membrane as were the other cationic drugs (Fig. 6). This suggested that P-glycoprotein should take up transport substrates from near the surface region of the membrane. Drugs are then free to diffuse laterally into the drug-binding chamber of P-glycoprotein (Fig. 7, *A* and *B*). The crystal structures of MsbA had a chamber that was open to the inner leaflet of the plasma membrane and further supports this notion (51,58). In our homology model, there are two obvious drug entry clefts at the correct height relative to the inner leaflet of the bilayer (Fig. 2 *A*, *front* and *back*; Figs. 7 and 8, *insets*). These drug entry clefts are similar but not identical to the drug entry ''gates'' proposed by Loo and Clarke (70). A similar cleft opening was observed in the two-dimensional crystal of P-glycoprotein (71).

The uncharged form of verapamil easily entered the hydrocarbon core of the lipid bilayer and abolished all polar interactions with the surface (Figs. 4 *A*, 5, *A* and *C*, and 6 *A*). On the other hand, the protonated form of verapamil (Figs. 4 *B*, 5, *B* and *D*, and 6 *B*) and SL-verapamil did not (Fig. 6 *D*). These results agree with the fact that the activation energy of dehydration is the primary determinant in passive membrane permeation (23). Hence the very large hydration energy of fixed-charge molecules (72) is too large to overcome for passive permeation through the membrane. This explains why the fixed positively charged SL-verapamil did not permeate the bilayer by flip-flopping in transport studies (21). A lipid bilayer is composed from well-ordered layers of different physical properties (73). To passively cross the membrane, a particle must pass through two highly charged headgroup layers, two hydrophobic layers near the membrane surfaces and through the hydrophobic tail zone (hydrophobic core). However, the physical properties of the drug-binding chamber are totally different from that of the lipid bilayer. The existence of both polar and hydrophobic residues inside the drug-binding chamber allows sequential drug dehydration, solvation, and rehydration to promote passage across the membrane by the ''solvation exchange mechanism'' described later. In this article, we use the terms hydration/dehydration to specify solvation/desolvation of the drug by water molecules. The terms solvation/desolvation alone imply interaction of the drug with any solvent that surrounds it, including the drug binding chamber of P-glycoprotein.

Drug binding to P-glycoprotein

Although P-glycoprotein can transport neutral drugs, it prefers positively charged compounds (Introduction). This suggests the presence of negatively charged residues near the drug-binding site. Based on the mutational and cross-linking studies, drug-binding sites are believed to be located in the transmembrane domain. However, there are no acidic residues in the middle of the drug-binding chamber of P-glycoprotein (Figs. 7 and 8). We proposed above that P-glycoprotein picks up substrates from the interfacial surface zone of the membrane. In agreement with this, there are four conserved acidic residues, namely D188, E353, E782, and D997 located in the surface zone within ICD helices (Figs. 7 and 8; see also Figs. 1 and 2). Similar acidic residues have been identified in the transport of cationic substrates in other drug resistance transporters (59,61,74–79). In P-glycoprotein, these acidic residues are close to the membrane surface and are accessible from within the chamber. They are also close to the drug entry clefts. Surrounding these residues are many polar and aromatic residues that may be necessary for drug interactions (Fig. 7). When drugs present at the membrane surface diffuse laterally into the drug binding chamber of P-glycoprotein, these acidic residues can provide the observed cation preference. It is in this zone that the initial interaction of P-glycoprotein and drugs occurs.

The involvement of ICD helices in initial drug binding is very important in the active transport mechanism. In the crystal structure of MsbA, ICD1 interacts with the Q-loop of N-terminal nucleotide binding domain (58). This Q-loop has a conserved glutamine residue that is thought to bind to a catalytic Mg^{2+} ion and a catalytic water molecule in some ABC proteins (80). In mouse P-glycoprotein, it has been shown that the primary role of the Q-loop glutamines is in interdomain signal communication between catalytic sites and drug-binding sites (81). A critical role of Q-loop and ICD1 helix interactions for conformational change transmission between the catalytic site and transmembrane domain was previously proposed (43). Binding of drugs at the ICD/transmembrane helices interface would lead to reorganization of the ICD helices and thus activate catalysis through ICD/Q-loop interactions. Similarly, ATP hydrolysis would induce the reorganization of the ICD helices coupled to the reorganization of the transmembrane helices to initiate the transport process. Recently, we found that G185 to valine mutation at the interface of ICD1 and TM3 altered the energy coupling of colchicine transport (33). In Results and Fig. 9 we demonstrate that G185V P-glycoprotein interacts with colchicine in a manner that removes an overabundance of nonpolar van der Waals interactions while satisfying the available H-bond acceptors. This is the molecular basis for the observed improved energy coupling and transport of colchicine. Thus, substitution of a low flexiblity valine for the highly flexible glycine disturbs the reorganization of ICD and transmembrane helices such that the binding-site for colchicine is constrained in a more favorable conformation for colchicine binding. Loo and Clarke reported rotation of helices 6 and 12 by ATP hydrolysis based on the cross-linking experiments (82). Because TM6 and TM12 are connected to ICD helices 3 and 6, respectively (Fig. 1), rotation of these transmembrane helices (as seen by Rothnie et al. (83)) inescapably indicates rotation of ICD helices 3 and 6. The postulated conserved drug interacting residues D353 and D997 are located in ICD3 and ICD6. As discussed previously, these residues may interact with positively charged drugs and any rotation of ICD helices would break such interactions. In addition, helix rotation allows breaking of hydrogen bonds between drug and polar residues such as S351 and Q347. Other ICDs and transmembrane helices, as well as ICD3, ICD6, TM6, and TM12, may rotate and break hydrogen and charged bonds between drugs and P-glycoprotein. Because such interactions tether the hydrophilic parts of the drug to the membrane interface zone of P-glycoprotein, breaking of these bonds could initiate flipping of drugs leading to eventually transport drugs to the other side of the membrane.

Solvation exchange mechanism

The most energetically costly step of membrane permeation of a polar particle is dehydration (23). For charged

molecules, the dehydration energy required is too high to overcome (72). For instance, the hydration energy of the charged form of methylamine was reported as ~280 kJ mol^{-1}. In the case of the KcsA potassium channel, a potassium ion in the selectivity filter was coordinated with eight carbonyl oxygens and two waters to minimize the hydration energy difference (84). The small hydration-energy difference of potassium ions between the water phase and the selectivity filter was an essential factor for the potassium channel functionality. P-glycoprotein must have a similar mechanism to transport polar and charged drugs. Based on these facts, we hypothesize that P-glycoprotein works as a hydration exchanger. In this mechanism, polar interactions of drugs with lipid headgroups or water are replaced by hydrogen bonds of polar side chains in the chamber and ICD helices (Fig. 10). Limited access of water and lipid headgroups to the drug binding sites facilitates the replacement of the hydration shell around the drugs by hydrogen bonds to P-glycoprotein. As discussed above, ATP hydrolysis rotates ICD and transmembrane helices to break hydrogen and charged bonds between drug and protein (Fig. 10 *C*). In addition to bonds breaking, the chamber cleft, open to the inner leaflet of plasma membrane, should be closed (Fig. 10 *C*). Further helix rotations create an open pore to other side of the membrane (Fig. 10 *D*). Part of the energy used in breaking drug to protein bonds would be compensated by newly formed favorable interactions with other polar residues and water inside the drug-binding chamber. Once the protein to drug H-bonds are disrupted, the previously interfacial region tethered drug will initiate flipping as it searches for new bonding partners (Fig. 10, *B–C*). This movement is facilitated by the presence of hydrophilic residues (Fig. 7) and of water molecules in the drug-binding chamber to allow transient compensating hydrogen bonds to form. Fluorescent maleimide accessibility tests of the drug-binding chamber of the bacterial multidrug transporter, LmrA, suggested an aqueous filled chamber (85). The high content of polar residues in the drug-binding chamber of P-glycoprotein (Fig. 7) suggests a similar aqueous filled chamber. It has been demonstrated that P-glycoprotein drug-binding chamber is accessible to water during the transport cycle (86). Brownian motion can then drive the drugs across the

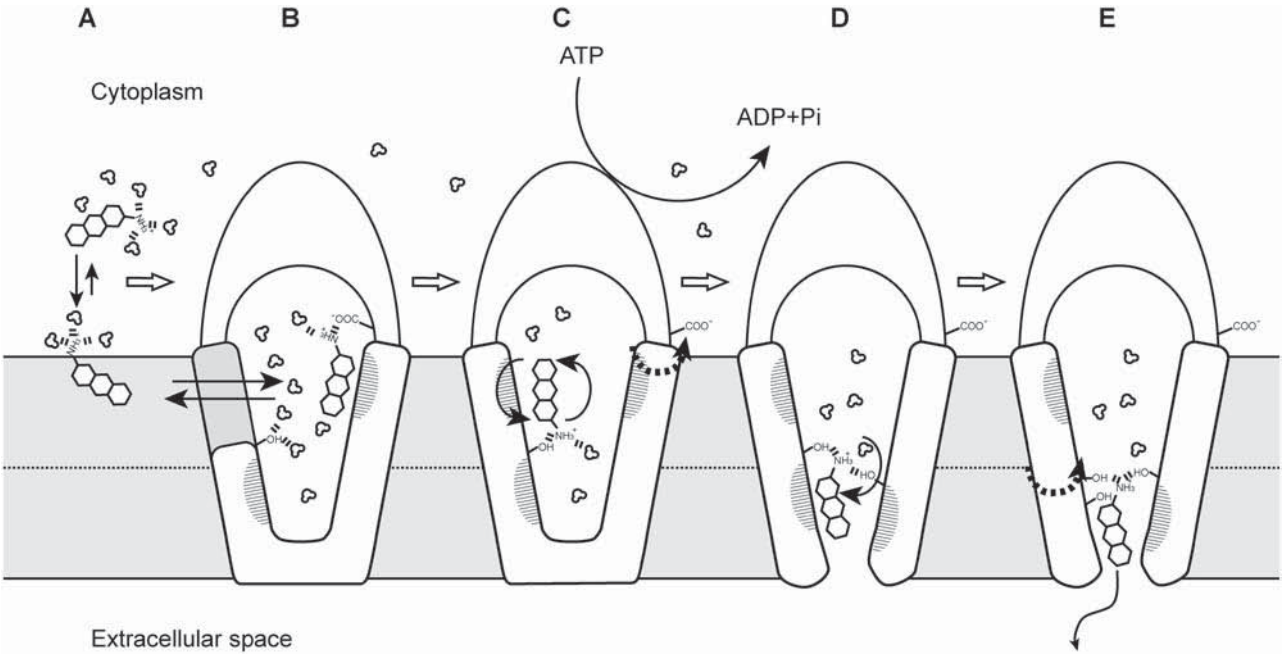

FIGURE 10 Solvation exchange mechanism of drug transport by P-glycoprotein. A postulated mechanism of drug transport by P-glycoprotein is illustrated. (*A*) A drug molecule is in equilibrium between the aqueous phase and the lipid bilayer. Due to hydrophobicity, drugs partition to the inner leaflet of the plasma membrane. Drugs maintain contact with water and lipid headgroups through polar interactions to the polar parts of the drug. (*B*) The drug molecule can laterally diffuse to the inside of the drug-binding chamber and bind to the drug-binding site. Part of the hydration shell of the drug is replaced by the polar residues in the intracellular domain helices (ICD helices) and the upper part of the drug-binding chamber. The hydrophobic part of the drug is adsorbed by hydrophobic residues in the chamber (*hatched areas*) through van der Waals interactions. (*C*) ATP hydrolysis closes the entry cleft and rotates helices located in the ICD and chamber domains and destroys electrostatic interactions and hydrogen bonds between the polar part of the drug and P-glycoprotein (*dotted arrow*). Loss of polar interactions that tether the polar part of the drug to the surface zone initiates flipping of drug (*solid arrows*). Hydrophilic residues scattered inside of the putative drug-binding chamber, and water molecules, may form transient hydrogen bonds to the drug aiding in the flipping process. (*D*) ATP hydrolysis also opens an exit through which water access is available. (*E*) Later favorable hydrophobic interactions to the drug are removed (*dotted arrow*) and more water enters the chamber. Drug is thus forcibly rehydrated and partitioned to the water phase allowing diffusion to the extracellular aqueous space (*solid arrow*). This large unfavorable utilization of energy is compensated by large favorable interactions formed in other parts of P-glycoprotein by the same helix rotating events. See text for further details.

chamber to the other side. During this migration, hydrophobic residues scattered throughout the inside of the drug-binding chamber would maintain nonpolar interactions with the hydrophobic part of the drug. Moving the drug across the drug binding chamber is thus likely an isoenergetic process (from the perspective of the drug's chemical potential).

An important finding by Seelig and Landwojtowicz (12) was that there was an inverse relationship between the air-water partition coefficient of a drug (K_{aw}; which is highly correlated with the corresponding lipid-water partition coefficient) and the apparent Michaelis-Menten complex (K_m^D) such that $K_m^D \times K_{aw} \sim 1$. In other words, the exchange of drugs between the lipid and P-glycoprotein drug-binding sites was approximately isoenergetic. Specificity and transport rates were dependent on specific drug-protein bond interactions being formed (12,52). These facts support the model proposed above. Furthermore, in the overall energy balance of P-glycoprotein, we previously demonstrated that there was adequate energy generated by the hydrolysis of a single ATP molecule to forcibly rehydrate a typical transport substrate that was bound (52). This is so because the drug is not fully dehydrated but is ''solvated'' by the protein. We also demonstrated that drug transport had high activation energies. Drug transport was facilitated by large entropic compensation of unfavorable enthalpic terms indicating a high degree of bond reordering and compensation. Furthermore, we demonstrated that different drugs form different types of bond interactions with P-glycoprotein during transport. In the movement of drugs across the protein, we also demonstrated that those drugs that required a high degree of bond reformation and compensation in their transport were more difficult for P-glycoprotein to transport (33,52). This transport difficulty was manifested by lower intrinsic transport turnover rates as well as lower overall thermodynamic efficiency. This inverse relationship between bond formation and rate of drug transport was also observed in Fig. 9 in this study. Such obstacles to transport could be suppressed by changing the local structure of P-glycoprotein by mutation to improve coupling efficiency of particular drugs through modified drug interactions. This was the case for the improved transport of colchicine by the G185V mutation (33) (Fig. 9). Utilizing purified P-glycoprotein reconstituted in defined proteoliposomes, we unequivocally demonstrated net active transport (''uphill transport'') of drugs (21). In the catalytic cycle, Pi release precedes drug release, which is followed by ADP release (87). Approximately 20 kJ mol^{-1} of nucleotide-binding energy is still stored in the complex after the dissociation of Pi and drug. Finally, we demonstrated that the overall rate-limiting step of P-glycoprotein, during transport, was a carrier reorientation step (52). These facts, taken together with the previous discussion and results presented in this article, lead us to suggest that the last step of drug transport (Fig. 10 *E*) entails further helix rotating events. It is the final step of drug release that would likely require an energy input. These helix rotations remove favorable hydrophobic interactions to the drug while allowing more water to enter the chamber. P-glycoprotein now adopts the ''low-affinity drug-unloading'' conformation (33,52). Drugs are forcibly rehydrated to aid in their partitioning into the extracellular aqueous medium. It is thus likely that P-glycoprotein pumps out water as it pumps out substrates, as was originally suggested by Zeuthen and Stein (88). Overall, the net energy gain by the transported drug would be supplied by the energy of ATP hydrolysis through helix rotation events. The large unfavorable utilization of energy is compensated to some extent by large favorable interactions formed in other parts of P-glycoprotein by these same helix-rotating events. With the dissociation of ADP, the protein relaxes to its ground state.

This work was supported by National Institutes of Health grant GM52502 to M.K.S.

REFERENCES

1. Gottesman, M. M., and I. Pastan. 1993. Biochemistry of multidrug resistance mediated by the multidrug transporter. *Annu. Rev. Biochem.* 62:385–427.
2. Borst, P., and R. O. Elferink. 2002. Mammalian ABC transporters in health and disease. *Annu. Rev. Biochem.* 71:537–592.
3. Ambudkar, S. V., C. Kimchi-Sarfaty, Z. E. Sauna, and M. M. Gottesman. 2003. P-glycoprotein: from genomics to mechanism. *Oncogene*. 22:7468–7485.
4. Leslie, E. M., R. G. Deeley, and S. P. Cole. 2005. Multidrug resistance proteins: role of P-glycoprotein, MRP1, MRP2, and BCRP (ABCG2) in tissue defense. *Toxicol. Appl. Pharmacol.* 204:216–237.
5. Senior, A. E., M. K. Al-Shawi, and I. L. Urbatsch. 1995. ATP hydrolysis by multidrug-resistance protein from Chinese hamster ovary cells. *J. Bioenerg. Biomembr.* 27:31–36.
6. Dean, M., and R. Allikmets. 2001. Complete characterization of the human ABC gene family. *J. Bioenerg. Biomembr.* 33:475–479.
7. Holland, I. B., and M. A. Blight. 1999. ABC-ATPases, adaptable energy generators fuelling transmembrane movement of a variety of molecules in organisms from bacteria to humans. *J. Mol. Biol.* 293:381–399.
8. Sharom, F. J. 1997. The P-glycoprotein efflux pump: how does it transport drugs. *J. Membr. Biol.* 160:161–175.
9. Seelig, A. 1998. A general pattern for substrate recognition by P-glycoprotein. *Eur. J. Biochem.* 251:252–261.
10. Ecker, G., M. Huber, D. Schmid, and P. Chiba. 1999. The importance of a nitrogen atom in modulators of multidrug resistance. *Mol. Pharmacol.* 56:791–796.
11. Pleban, K., A. Macchiarulo, G. Costantino, R. Pellicciari, P. Chiba, and G. F. Ecker. 2004. Homology model of the multidrug transporter LmrA from *Lactococcus lactis*. *Bioorg. Med. Chem. Lett.* 14:5823–5826.
12. Seelig, A., and E. Landwojtowicz. 2000. Structure-activity relationship of P-glycoprotein substrates and modifiers. *Eur. J. Pharm. Sci.* 12:31–40.
13. Greenberger, L. M., C. J. Lisanti, J. T. Silva, and S. B. Horwitz. 1991. Domain mapping of the photoaffinity drug-binding sites in P-glycoprotein encoded by mouse mdr1b. *J. Biol. Chem.* 266:20744–20751.
14. Pleban, K., S. Kopp, E. Csaszar, M. Peer, T. Hrebicek, A. Rizzi, G. F. Ecker, and P. Chiba. 2005. P-glycoprotein substrate binding domains are located at the transmembrane domain/transmembrane domain interfaces: a combined photoaffinity labeling-protein homology modeling approach. *Mol. Pharmacol.* 67:365–374.
15. Loo, T. W., and D. M. Clarke. 1993. Functional consequences of phenylalanine mutations in the predicted transmembrane domain of P-glycoprotein. *J. Biol. Chem.* 268:19965–19972.

16. Ambudkar, S. V., S. Dey, C. A. Hrycyna, M. Ramachandra, I. Pastan, and M. M. Gottesman. 1999. Biochemical, cellular, and pharmacological aspects of the multidrug transporter. *Annu. Rev. Pharmacol. Toxicol.* 39:361–398.

17. Shapiro, A. B., A. B. Corder, and V. Ling. 1997. P-glycoprotein-mediated Hoechst 33342 transport out of the lipid bilayer. *Eur. J. Biochem.* 250:115–121.

18. Shapiro, A. B., and V. Ling. 1997. Extraction of Hoechst 33342 from the cytoplasmic leaflet of the plasma membrane by P-glycoprotein. *Eur. J. Biochem.* 250:122–129.

19. Shapiro, A. B., and V. Ling. 1998. Transport of LDS-751 from the cytoplasmic leaflet of the plasma membrane by the rhodamine-123-selective site of P-glycoprotein. *Eur. J. Biochem.* 254:181–188.

20. Bolhuis, H., H. W. van Veen, D. Molenaar, B. Poolman, A. J. Driessen, and W. N. Konings. 1996. Multidrug resistance in *Lactococcus lactis*: evidence for ATP-dependent drug extrusion from the inner leaflet of the cytoplasmic membrane. *EMBO J.* 15:4239–4245.

21. Omote, H., and M. K. Al-Shawi. 2002. A novel electron paramagnetic resonance approach to determine the mechanism of drug transport by P-glycoprotein. *J. Biol. Chem.* 277:45688–45694.

22. Bassolino-Klimas, D., H. E. Alper, and T. R. Stouch. 1993. Solute diffusion in lipid bilayer membranes: an atomic level study by molecular dynamics simulation. *Biochemistry.* 32:12624–12637.

23. Marrink, S. J., and H. J. C. Berendsen. 1996. Permeation process of small molecules across lipid membranes studied by molecular dynamics simulations. *J. Phys. Chem.* 100:16729–16738.

24. Shepherd, C. M., H. J. Vogel, and D. P. Tieleman. 2003. Interactions of the designed antimicrobial peptide MB21 and truncated dermaseptin S3 with lipid bilayers: molecular-dynamics simulations. *Biochem. J.* 370:233–243.

25. van Aalten, D. M., R. Bywater, J. B. Findlay, M. Hendlich, R. W. Hooft, and G. Vriend. 1996. PRODRG, a program for generating molecular topologies and unique molecular descriptors from coordinates of small molecules. *J. Comput. Aided Mol. Des.* 10:255–262.

26. Stewart, J. J. 1990. MOPAC: a semiempirical molecular orbital program. *J. Comput. Aided Mol. Des.* 4:1–105.

27. Tieleman, D. P., and H. J. C. Berendsen. 1996. Molecular dynamics simulations of a hydrated dipalmitoylphosphatidylcholine bilayer with different macroscopic boundary conditions and parameters. *J. Chem. Phys.* 105:4871–4880.

28. Berger, O., O. Edholm, and F. Jahnig. 1997. Molecular dynamics simulations of a fluid bilayer of dipalmitoylphosphatidylcholine at full hydration, constant pressure, and constant temperature. *Biophys. J.* 72:2002–2013.

29. Berendsen, H. J. C., D. van der Spoel, and R. van Drunen. 1995. GROMACS: a message-passing parallel molecular dynamics implementation. *Comput. Phys. Commun.* 91:43–56.

30. Lindahl, E., B. Hess, and D. van der Spoel. 2001. GROMACS 3.0: a package for molecular simulation and trajectory analysis. *J. Mol. Model.* [*Online*]. 7:306–317.

31. Hess, B., H. Bekker, H. J. C. Berendsen, and J. G. E. M. Fraaije. 1997. LINCS: a linear constraint solver for molecular simulations. *J. Comput. Chem.* 18:1463–1472.

32. Sali, A., and T. L. Blundell. 1993. Comparative protein modelling by satisfaction of spatial restraints. *J. Mol. Biol.* 234:779–815.

33. Omote, H., R. A. Figler, M. K. Polar, and M. K. Al-Shawi. 2004. Improved energy coupling of human P-glycoprotein by the glycine 185 to valine mutation. *Biochemistry.* 43:3917–3928.

34. Campbell, J. D., P. C. Biggin, M. Baaden, and M. S. Sansom. 2003. Extending the structure of an ABC transporter to atomic resolution: modeling and simulation studies of MsbA. *Biochemistry.* 42:3666–3673.

35. Thompson, J. D., D. G. Higgins, and T. J. Gibson. 1994. CLUSTAL W: improving the sensitivity of progressive multiple sequence alignment through sequence weighting, position-specific gap penalties and weight matrix choice. *Nucleic Acids Res.* 22:4673–4680.

36. Rost, B., and C. Sander. 1993. Prediction of protein secondary structure at better than 70% accuracy. *J. Mol. Biol.* 232:584–599.

37. Rost, B. 1996. PHD: predicting one-dimensional protein structure by profile-based neural networks. *Methods Enzymol.* 266:525–539.

38. Chang, G. 2003. Structure of MsbA from *Vibrio cholera*: a multidrug resistance ABC transporter homolog in a closed conformation. *J. Mol. Biol.* 330:419–430.

39. Hung, L. W., I. X. Wang, K. Nikaido, P. Q. Liu, G. F. Ames, and S. H. Kim. 1998. Crystal structure of the ATP-binding subunit of an ABC transporter. *Nature.* 396:703–707.

40. Laskowski, R. A., M. W. Macarthur, D. S. Moss, and J. M. Thornton. 1993. PROCHECK: a program to check the stereochemical quality of protein structures. *J. App. Crystallogr.* 26:283–291.

41. Gaudet, R., and D. C. Wiley. 2001. Structure of the ABC ATPase domain of human TAP1, the transporter associated with antigen processing. *EMBO J.* 20:4964–4972.

42. Ramachandran, G. N., and V. Sasisekharan. 1968. Conformation of polypeptides and proteins. *Adv. Protein Chem.* 23:283–438.

43. Locher, K. P., A. T. Lee, and D. C. Rees. 2002. The *E. coli* BtuCD structure: a framework for ABC transporter architecture and mechanism. *Science.* 296:1091–1098.

44. Davidson, A. L., and J. Chen. 2004. ATP-binding cassette transporters in bacteria. *Annu. Rev. Biochem.* 73:241–268.

45. Seigneuret, M., and A. Garnier-Suillerot. 2003. A structural model for the open conformation of the mdr1 P-glycoprotein based on the MsbA crystal structure. *J. Biol. Chem.* 278:30115–30124.

46. Stenham, D. R., J. D. Campbell, M. S. Sansom, C. F. Higgins, I. D. Kerr, and K. J. Linton. 2003. An atomic detail model for the human ATP binding cassette transporter P-glycoprotein derived from disulfide cross-linking and homology modeling. *FASEB J.* 17:2287–2289.

47. Shilling, R. A., L. Balakrishnan, S. Shahi, H. Venter, and H. W. van Veen. 2003. A new dimer interface for an ABC transporter. *Int. J. Antimicrob. Agents.* 22:200–204.

48. Higgins, C. F., and K. J. Linton. 2004. The ATP switch model for ABC transporters. *Nat. Struct. Mol. Biol.* 11:918–926.

49. Loo, T. W., M. C. Bartlett, and D. M. Clarke. 2004. Val133 and Cys137 in transmembrane segment 2 are close to residues Arg935 and Gly939 in transmembrane segment 11 of human P-glycoprotein. *J. Biol. Chem.* 279:18232–18238.

50. Loo, T. W., M. C. Bartlett, and D. M. Clarke. 2004. Disulfide cross-linking analysis shows that transmembrane segments 5 and 8 of human P-glycoprotein are close together on the cytoplasmic side of the membrane. *J. Biol. Chem.* 279:7692–7697.

51. Reyes, C. L., and G. Chang. 2005. Structure of the ABC transporter MsbA in complex with ADP.vanadate and lipopolysaccharide. *Science.* 308:1028–1031.

52. Al-Shawi, M. K., M. K. Polar, H. Omote, and R. A. Figler. 2003. Transition state analysis of the coupling of drug transport to ATP hydrolysis by P-glycoprotein. *J. Biol. Chem.* 278:52629–52640.

53. Demeule, M., J. Jodoin, D. Gingras, and R. Beliveau. 2000. P-glycoprotein is localized in caveolae in resistant cells and in brain capillaries. *FEBS Lett.* 466:219–224.

54. Eytan, G. D., and P. W. Kuchel. 1999. Mechanism of action of P-glycoprotein in relation to passive membrane permeation. *Int. Rev. Cytol.* 190:175–250.

55. Reuter, G., T. Janvilisri, H. Venter, S. Shahi, L. Balakrishnan, and H. W. Van Veen. 2003. The ATP-binding cassette multidrug transporter LmrA and lipid transporter MsbA have overlapping substrate specificities. *J. Biol. Chem.* 278:35193–35198.

56. Ruetz, S., and P. Gros. 1994. Phosphatidylcholine translocase: a physiological role for the mdr2 gene. *Cell.* 77:1071–1081.

57. Yang, A. S., and B. Honig. 2000. An integrated approach to the analysis and modeling of protein sequences and structures. II. On the relationship between sequence and structural similarity for proteins that are not obviously related in sequence. *J. Mol. Biol.* 301:679–689.

58. Chang, G., and C. B. Roth. 2001. Structure of MsbA from *E. coli*: a homolog of the multidrug resistance ATP binding cassette (ABC) transporters. *Science*. 293:1793–1800.

59. Shilling, R., L. Federici, F. Walas, H. Venter, S. Velamakanni, B. Woebking, L. Balakrishnan, B. Luisi, and H. W. van Veen. 2005. A critical role of a carboxylate in proton conduction by the ATP-binding cassette multidrug transporter LmrA. *FASEB J*. 19:1698–1700.

60. Pajeva, I. K., and M. Wiese. 2002. Pharmacophore model of drugs involved in P-glycoprotein multidrug resistance: explanation of structural variety (hypothesis). *J. Med. Chem*. 45:5671–5686.

61. Yu, E. W., G. McDermott, H. I. Zgurskaya, H. Nikaido, and D. E. Koshland. 2003. Structural basis of multiple drug-binding capacity of the AcrB multidrug efflux pump. *Science*. 300:976–980.

62. Seelig, A., X. Li Blatter, and F. Wohnsland. 2000. Substrate recognition by P-glycoprotein and by the multidrug resistance-associated protein MRP1: a comparison. *Eur. J. Pharm. Sci*. 12:31–40.

63. Qu, Q., and F. J. Sharom. 2002. Proximity of bound Hoechst 33342 to the ATPase catalytic sites places the drug binding site of P-glycoprotein within the cytoplasmic membrane leaflet. *Biochemistry*. 41:4744–4752.

64. Lugo, M. R., and F. J. Sharom. 2005. Interaction of LDS-751 with P-glycoprotein and mapping of the location of the R drug binding site. *Biochemistry*. 44:643–655.

65. Seelig, A., and E. Gatlik-Landwojtoxicz. 2005. Biophysical characterization of inhibitors of multidrug efflux transporters: their membrane and protein interactions. *Mini Rev. Med. Chem*. 5:135–151.

66. Romsicki, Y., and F. J. Sharom. 1999. The membrane lipid environment modulates drug interactions with the P-glycoprotein multidrug transporter. *Biochemistry*. 38:6887–6896.

67. de Wolf, F. A., M. Maliepaard, F. van Dorsten, I. Berghuis, K. Nicolay, and B. de Kruijff. 1990. Comparable interaction of doxorubicin with various acidic phospholipids results in changes of lipid order and dynamics. *Biochim. Biophys. Acta*. 1096:67–80.

68. Chow, A., J. Kennedy, R. Pottier, and T. Truscott. 1986. Rhodamine 123: photophysical and photochemical properties. *Photobiochem. Photobiophys*. 11:139–148.

69. Ferguson, M. W., P. C. Beaumont, S. E. Jones, S. Navaratnam, and B. J. Parsons. 1999. Excited state and free radical properties of Rhodamine 123: a laser flash photolysis and radiolysis study. *Phys. Chem. Chem. Phys*. 1:261–268.

70. Loo, T. W., and D. M. Clarke. 2005. Do drug substrates enter the common drug-binding pocket of P-glycoprotein through ''gates''? *Biochem. Biophys. Res. Commun*. 329:419–422.

71. Rosenberg, M. F., A. B. Kamis, R. Callaghan, C. F. Higgins, and R. C. Ford. 2003. Three-dimensional structures of the mammalian multidrug resistance P-glycoprotein demonstrate major conformational changes in the transmembrane domains upon nucleotide binding. *J. Biol. Chem*. 278:8294–8299.

72. Pepe, G., G. Guiliani, S. Loustalet, and P. Halfon. 2002. Hydration free energy a fragmental model and drug design. *Eur. J. Med. Chem*. 37:865–872.

73. Marrink, S. J., and H. J. C. Berendsen. 1994. Simulation of water transport through a lipid membrane. *J. Phys. Chem*. 98:4155–4168.

74. Zhang, D. W., H. M. Gu, D. Situ, A. Haimeur, S. P. Cole, and R. G. Deeley. 2003. Functional importance of polar and charged amino acid residues in transmembrane helix 14 of multidrug resistance protein 1 (MRP1/ABCC1): identification of an aspartate residue critical for conversion from a high to low affinity substrate binding state. *J. Biol. Chem*. 278:46052–46063.

75. Yerushalmi, H., and S. Schuldiner. 2000. An essential glutamyl residue in EmrE, a multidrug antiporter from *Escherichia coli*. *J. Biol. Chem*. 275:5264–5269.

76. Edgar, R., and E. Bibi. 1999. A single membrane-embedded negative charge is critical for recognizing positively charged drugs by the *Escherichia coli* multidrug resistance protein MdfA. *EMBO J*. 18: 822–832.

77. Brown, M. H., and R. A. Skurray. 2001. Staphylococcal multidrug efflux protein QacA. *J. Mol. Microbiol. Biotechnol*. 3:163–170.

78. Tamura, N., S. Konishi, and A. Yamaguchi. 2003. Mechanisms of drug/H+ antiport: complete cysteine-scanning mutagenesis and the protein engineering approach. *Curr. Opin. Chem. Biol*. 7:570–579.

79. Otsuka, M., M. Yasuda, Y. Morita, C. Otsuka, T. Tsuchiya, H. Omote, and Y. Moriyama. 2005. Identification of essential amino acid residues of the NorM Na+/multidrug antiporter in *Vibrio parahaemolyticus*. *J. Bacteriol*. 187:1552–1558.

80. Hopfner, K. P., A. Karcher, D. S. Shin, L. Craig, L. M. Arthur, J. P. Carney, and J. A. Tainer. 2000. Structural biology of Rad50 ATPase: ATP-driven conformational control in DNA double-strand break repair and the ABC-ATPase superfamily. *Cell*. 101:789–800.

81. Urbatsch, I. L., K. Gimi, S. Wilke-Mounts, and A. E. Senior. 2000. Investigation of the role of glutamine-471 and glutamine-1114 in the two catalytic sites of P-glycoprotein. *Biochemistry*. 39:11921–11927.

82. Loo, T. W., and D. M. Clarke. 2001. Cross-linking of human multidrug resistance P-glycoprotein by the substrate, Tris-(2-maleimidoethyl)-amine, is altered by ATP hydrolysis. *J. Biol. Chem*. 276:31800–31805.

83. Rothnie, A., J. Storm, J. Campbell, K. J. Linton, I. D. Kerr, and R. Callaghan. 2004. The topography of transmembrane segment six is altered during the catalytic cycle of P-glycoprotein. *J. Biol. Chem*. 279:34913–34921.

84. Morais-Cabral, J. H., Y. Zhou, and R. MacKinnon. 2001. Energetic optimization of ion conduction rate by the K+ selectivity filter. *Nature*. 414:37–42.

85. Poelarends, G. J., and W. N. Konings. 2002. The transmembrane domains of the ABC multidrug transporter LmrA form a cytoplasmic exposed, aqueous chamber within the membrane. *J. Biol. Chem*. 277: 42891–42898.

86. Loo, T. W., M. C. Bartlett, and D. M. Clarke. 2004. The drug-binding pocket of the human multidrug resistance P-glycoprotein is accessible to the aqueous medium. *Biochemistry*. 43:12081–12089.

87. Senior, A. E., M. K. Al-Shawi, and I. L. Urbatsch. 1995. The catalytic cycle of P-glycoprotein. *FEBS Lett*. 377:285–289.

88. Zeuthen, T., and W. D. Stein. 1994. Cotransport of salt and water in membrane proteins: membrane proteins as osmotic engines. *J. Membr. Biol*. 137:179–195.

89. Kraulis, P. J. 1991. MOLSCRIPT:A program to produce both detailed and schematic plots of protein structures. *J. App. Crystallogr*. 24: 946–950.